AIAA JOURNAL
Vol. 48, No. 11, November 2010

Transient Separation Control Using Pulse-Combustion Actuation

Daniel P. Brzozowski,* George T. K. Woo,* John R. Culp,* and Ari Glezer*
Georgia Institute of Technology, Atlanta, Georgia 30332

DOI: 10.2514/1.45904

The transitory response of the flow over a stalled, two-dimensional (NACA 4415) airfoil to pulsed actuation on time scales that are an order of magnitude shorter than the characteristic convective time scale is investigated experimentally ($Re = 570,000$). Actuation is effected by momentary [$\mathcal{O}$(1 ms)] pulsed jets that are generated by a spanwise array of combustion-based actuators integrated into the center section of the airfoil. The flowfield in the cross-stream plane above the airfoil and in its near wake is computed from multiple high-resolution particle image velocity images that are obtained phase locked to the actuation waveform and allow for tracking of vorticity concentrations. The brief actuation pulse leads to a remarkably strong transitory change in the circulation about the entire airfoil that is manifested by a severing of the separated vorticity layer and the subsequent shedding of a large-scale clockwise vortex that forms the separated flow domain. The clockwise severed vorticity layer that follows behind this detached vortex has a distinct sharp streamwise edge that grows and rolls up as the layer is advected along the surface. It is shown that the shedding of the severed vortex and the accumulation of surface vorticity are accompanied by a transitory increase in the magnitude of the circulation about the airfoil that lasts 8–10 convective time scales. The attached vorticity layer ultimately lifts off the surface in a manner that is reminiscent of dynamic stall, and the flow separates again.

I. Introduction

TRADITIONAL aerodynamic flow-control techniques for suppressing flow separation over stalled airfoils have relied primarily on the flow receptivity to actuation within a narrow frequency band that is dominated by strong coupling to the instability of the near wake (e.g., Wu et al. [1]). In this approach, which has been exploited with varying degrees of success since the early 1980s, the actuation period scales with the advection time over the length of the separated flow domain (or the width of the wake) such that the dimensionless actuation frequency $St_{\text{act}} \sim \mathcal{O}(1)$ and lift enhancement are achieved by Coanda-like deflection of the separated shear layer toward the surface (e.g., Ahuja and Burrin [2], Neuburger and Wygnanski [3], Seifert et al. [4], Tuck and Soria [5], and Sosa et al. [6]). In addition, a number of numerical (Wu et al. [1], Wake and Lurie [7], Duraisamy and Baeder [8], and Florea and Wake [9]) and experimental (Lorber et al. [10,11], and Greenblatt and Wygnanski [12]) investigations employed time-periodic actuation in an effort to manipulate dynamic stall on oscillating airfoils, and they have shown that the actuation can increase the unsteady stall angles and poststall lift.

A different approach for reducing flow separation, which is decoupled from the global flow (wake) instabilities, modifies the apparent aerodynamic shape of the surface and, thereby, the streamwise pressure gradient upstream of separation. Actuation is effected by forming a controlled interaction domain of trapped vorticity between a surface-mounted fluidic actuator (e.g., a synthetic jet; Smith and Glezer [13]) and the crossflow above the surface (e.g., Honohan et al. [14]). Broadband control is attained at actuation frequencies that are at least an order of magnitude higher than the characteristic wake frequency [i.e., $St_{\text{act}} \sim \mathcal{O}(10)$] and are therefore decoupled from global flow instabilities (Amitay et al. [15], Amitay and Glezer [16], and Glezer et al. [17]).

The receptivity and unsteadiness of the separated flow domain over stalled airfoils has been exploited to affect quasi-steady or transitory aerodynamic forces using anharmonic or temporally modulated actuation. Amitay and Glezer [16,18,19] investigated flow transients associated with the onset and termination of high-frequency actuation that lead to flow attachment over a stalled airfoil, and they noted the similarity to the transients that accompany separation and attachment during dynamic stall. In particular, Amitay and Glezer [19] demonstrated that the separated flow is extremely susceptible to transitory actuation, and they showed that when the actuation input was applied on time scales that are significantly shorter than the characteristic advection time over the separated flow domain, the resulting aerodynamic forces are larger than the forces realized by conventional, continuous time-harmonic actuation. The onset and termination of continuous actuation over a flat-plate flap configuration were investigated by Darabi and Wygnanski [20,21], who reported close characteristic attachment and separation times for optimal actuation momentum coefficient C_μ and dimensionless frequency F^+. More recently, Siauw et al. [22] investigated the transient attachment and separation on a NACA 0015 airfoil using fluidic vortex generators and, similarly, Mathis et al. [23] considered transient attachment and separation by pneumatic disruption of an actuation jet that effects separation over a splitter plate when active.

The utility of pulsed actuation for separation control was demonstrated by Crittenden et al. [24–26] and Funk et al. [27], who used time-periodic momentary [$\mathcal{O}$(1 ms)] high-impulse actuation jets produced by combustion-powered actuation (COMPACT). This work was later extended by Brzozowski and Glezer [28] to the investigation of the transitory response of the flow over a stalled NACA 4415 airfoil to actuation by a single pulse having a characteristic time scale of $0.05T_{\text{conv}}$. These authors showed that the momentary actuation leads to a partial collapse of the separated flow domain coupled with a momentary increase in circulation magnitude on a time scale that is nearly $10T_{\text{conv}}$. In subsequent investigations, Woo et al. [29,30] and Woo and Glezer [31] showed that successive actuation by single-pulse or short actuation bursts results in a rapid buildup of circulation that can extend the streamwise domain of the attached boundary layer toward the trailing edge. The fast dynamic response associated with the reattachment process, combined with the relatively long relaxation process, allows low duty cycle pulsed actuation bursts to prevent full stall between bursts.

The present paper focuses on the receptivity of separated flow over a stalled airfoil to a single, brief actuation pulse, with specific emphasis on the severing and detachment of the separated vorticity layer, the subsequent collapse of the separated flow domain, and the concomitant accumulation of vorticity on the surface of the airfoil as the upstream boundary layer becomes attached. Of particular note are

Presented as Paper 2006-3024 at the 3rd AIAA Flow Control Conference, San Francisco, CA, 5–8 June 2006; received 9 June 2009; revision received 23 June 2010; accepted for publication 27 June 2010.

*George W. Woodruff School of Mechanical Engineering.

the transitory change and increase in the magnitude of the circulation about the entire airfoil that last for 8–10 convective time scales.

II. Experimental Apparatus and Procedure

A. Airfoil Model

The present experiments use a two-dimensional (2-D) airfoil model with a fixed cross section that is based on a NACA 4415 configuration, as shown in Fig. 1a, including the coordinate system in the airfoil's frame of reference (x, y), for which the origin coincides with the leading edge. The experiments are conducted in an open return wind tunnel where the model spans the entire width of the 1×1 m wind-tunnel test section and has a chord length of $c = 457$ mm and a maximum thickness-to-chord ratio of $t/c = 0.15$. The airfoil is divided into three spanwise segments (Fig. 1b) by means of fences, having a maximum chordwise length and height (normal to the chord) of $1.3c$ and $0.44c$, respectively, to maintain a nominally 2-D flow over the center section of the airfoil (which comprises 21% of the total span). The center segment is instrumented with a circumferential array of 75 pressure ports (located at midspan) that are each connected to an external high-speed pressure measurement system (the uncertainty of the time-averaged pressure measurements is estimated to be less than 1%). The present experiments are conducted at a freestream speed of $U_0 = 20$ m/s; the corresponding Reynolds number (based on the airfoil chord, c) is $Re_c = 570,000$, and the flow's convective time scale over the airfoil is $T_{\text{conv}} = 25$ ms.

As shown in Fig. 2a, in the absence of actuation, the center segment begins to stall at $\alpha \approx 16°$ (which is higher than the nominal stall angle of $\alpha \approx 12°$ at $Re_c = 3 \cdot 10^6$; Abbot and von Doenhoff [32]). It is noted that the boundary layer on the model appears to be turbulent. The bulk of the present measurements are obtained at $\alpha = 19°$, for which $C_L = 1.33$ and $C_D = 0.21$. The corresponding circumferential pressure distribution is shown in Fig. 2b and, as evident from these data, the peak pressure on the suction side of the airfoil, $C_p = -4.36$, occurs at $x/c = 0.004$ and is followed by an adverse pressure gradient, and the flow subsequently separates at $x/c \approx 0.3$ (the actuator jets are located at $x/c = 0.2$).

B. Combustion Actuator

The airfoil's center segment is equipped with a modular spanwise array of seven individually addressable, adjacent combustion-based jet actuators that span its entire width (the two outboard segments are unactuated). COMPACT technology exploits the chemical energy of a gaseous fuel/oxidizer mixture, which is ignited within a miniature [$\mathcal{O}(1\ \text{cm}^3)$] combustion chamber to create a high-pressure pulse and, consequently, a momentary high-momentum jet of exhaust products that forms through an integrated orifice (in the present experiments, the actuators are operated in concert). The momentary jets that reach supersonic speed at the orifice are formed by the ignition of a (nonpremixed) mixture of air and hydrogen, using miniature spark plugs driven by a computer-controlled electronic ignition system.

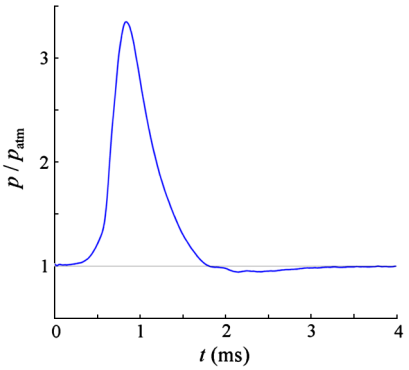

Fig. 3 Phase-averaged chamber pressure following ignition at $t = 0$ with an equivalence ratio of 0.8 (Woo et al. [30]).

Figure 3 shows phase-averaged measurements of the chamber pressure ratio, $p_r = p/p_{\text{atm}}$, following ignition with an equivalence ratio of 0.8. It is evident that the combustion leads to a sharp pressure peak, which then decreases to atmospheric pressure within 2–3 ms following ignition. The characteristics of the pressure pulse (i.e., amplitude, duration, etc.) are governed by a balance between the heat release and pressure rise from the combustion process (which are affected by the fuel type, mixture ratio, and flame propagation properties), and the subsequent decrease in pressure occurs due to the jet flow and heat transfer to the combustor walls. The flow of fuel and oxidizer into the chamber is typically regulated by small passive fluidic elements that exploit the pressure rise within the chamber to shut off the inlet flow. When the pressure within the chamber falls below the supply pressure, fresh reactants flow into the chamber, displacing the remaining exhaust gases and filling the chamber for the next actuation pulse. The actuation repetition rate is set by the

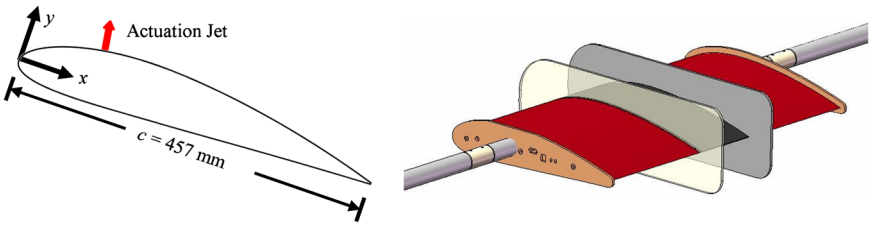

Fig. 1 Airfoil model with the integrated combustion actuator: a) NACA 4415 profile with coordinate systems and the position of the actuation jet and b) CAD rendering of the three-dimensional wind-tunnel model, where the active (center) section is separated from the outboard sections with fences (Woo and Glezer [31]).

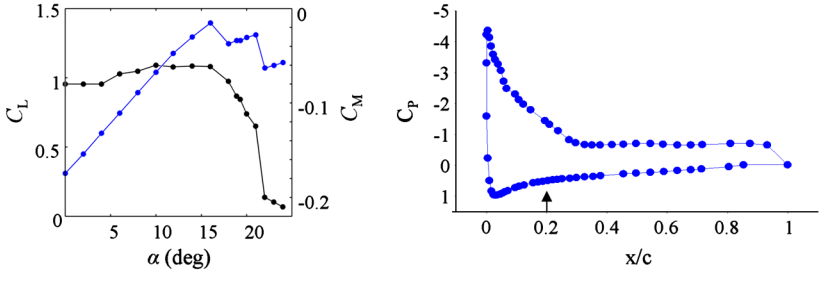

Fig. 2 Baseline steady-state airfoil performance: a) static variation in C_L and C_M with α and b) pressure distribution over the stalled airfoil at $\alpha = 19°$.

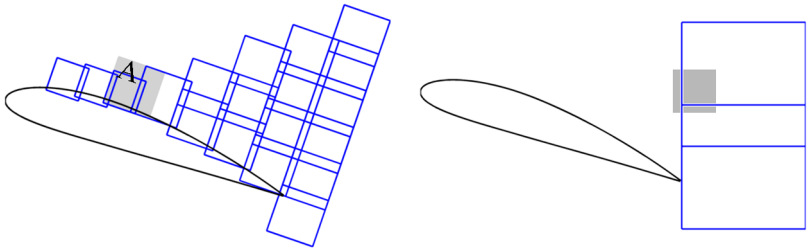

a) b)

Fig. 4 Map of PIV frames: a) global measurements with time-resolved window shaded and b) wake measurements with long-time window shaded.

ignition and is continuously variable with an upper limit that is set by the characteristic duration of the high-pressure pulse within the chamber and the reactants' refill and mixing times.

In the present configuration, each jet emanates normal to the airfoil's surface from a rectangular orifice, located at $x/c = 0.2$, that is flush mounted in the surface. The (spanwise) length and (streamwise) width of the rectangular orifice of each actuation are $l = 19$ and $w = 0.18$ mm, respectively, and the spacing between adjacent orifices is 3.2 mm. Because of the small spacing between adjacent orifices, the actuation jets merge rapidly as they are advected in the streamwise direction (the characteristic convective streamwise scale of the actuation jets is about $111w$ compared with their spanwise gap of $18w$). Furthermore, edge effects are minimal since (as demonstrated in schlieren visualization) the jets develop small-scale three-dimensional motions within a few orifice widths; therefore, the actuation is nearly spanwise uniform across the active segment of the airfoil.

C. Particle Image Velocimetry

The flow over the airfoil is characterized using phase-locked particle image velocimetry (PIV) in the cross-stream plane $z = 0$. The flow is seeded with micron-sized smoke particles (using a commercial fog machine, where the nominal particle diameter d is 50 μm) and is illuminated using a double-pulse neodymium-doped yttrium aluminum garnet laser. Image pairs are captured using a 1008×1016 pixel charge-coupled device camera that is mounted on a two-axis (computer controlled) traversing mechanism. Phase-averaged maps of the resulting flowfield are composed of 19 individual frames that are shown schematically in Fig. 4. At each frame, sets of PIV images are captured at a sequence of predetermined time delays relative to the actuation pulse. Data sets over the airfoil include 250 image pairs, and data sets across the wake include 200 image pairs (the mean velocity estimates converge over this number of realizations). While the bulk of the images are obtained at a spatial resolution of 73 μm/pixel, several higher-resolution views (shown in smaller frames) are taken at 50 μm/pixel. An additional frame (A, marked in gray) is used to provide additional detail of the dynamics of the onset of flow attachment. The frames across the wake of the airfoil (near its trailing edge) are recorded with a resolution of 200 μm/pixel and used to assess the time-dependent circulation about the airfoil. The uncertainties in PIV measurements are based on the analysis of Adrian [33] and Westerweel [34]. The time-averaged and phase-averaged velocities are computed from 200, 250, and 450 realizations in the wake, full-field, and high-magnification fields, respectively, yielding uncertainties of less than 1%.

III. Transitory Control of Aerodynamic Performance

As discussed in Sec. I, the objective of the present work is to exploit the receptivity of the separated flow over a stalled airfoil to pulse actuation that gives rise to transitory flow attachment, large-scale changes in vorticity accumulation and flux and, consequently, changes in the global circulation.

The baseline (stalled) flow is shown in time-averaged raster plots of concentrations of the normalized spanwise vorticity (Fig. 5a), $\hat{\omega}_z = \omega_z \cdot T_{\text{conv}}$ (where $T_{\text{conv}} = c/U_0$ is the convective time scale over the airfoil, and ω_z is the spanwise vorticity) and of the velocity magnitude (Fig. 5b), $\hat{v} = \sqrt{u^2 + v^2}/U_0$ (where u and v are the streamwise and cross-stream velocities, respectively). The extent of the separated flow domain is evident from the vorticity concentrations. The boundary layer separates around $x/c \approx 0.3$ (cf., Fig. 2), and a large recirculation flow domain forms over the top surface of the airfoil, having a cross-stream extent of nominally $0.3c$ near the trailing edge. It is noteworthy that the reversed (recirculating) flow leads to the formation of counterclockwise (CCW) vorticity concentrations near the surface of the airfoil. The raster plots of the velocity magnitude show that, within the separated flow domain, the peak recirculating velocity is lower than the freestream velocity (about $0.8U_0$), while the speed immediately above the separated domain is about 30% larger than the freestream velocity. It is also noteworthy that, upstream of separation, the speed of the outer flow above the airfoil is almost $2U_0$.

The dynamics of the separated flow domain are drastically altered when actuation is applied. This is shown in a sequence of raster plots of $\hat{\omega}_z$ and $\hat{v}$, taken at $t/T_{\text{conv}} = 0$, 0.2, 0.4, 0.6, 0.8, 1, 1.4, 2, and 3.8 following the actuation, that is shown in Figs. 6a–6i, respectively.

The actuation is applied at $t/T_{\text{conv}} = 0$ and, as noted in Sec. II, the characteristic impulse duration is $\mathcal{O}(0.05T_{\text{conv}})$. The phase-averaged recording in Fig. 6a is triggered at actuation and is therefore similar to the time-averaged flowfield in Fig. 5a. By $t/T_{\text{conv}} = 0.2$ (Fig. 6b), there is a noticeable discontinuity in the vorticity along the surface near the point of separation ($x/c = 0.3$), and by $t/T_{\text{conv}} = 0.4$ (Fig. 6c), the separating shear layer appears to be severed from the upstream boundary layer. In fact, the raster plot of $\hat{v}$ shows a protrusion of low-speed fluid (from the separated flow domain) into

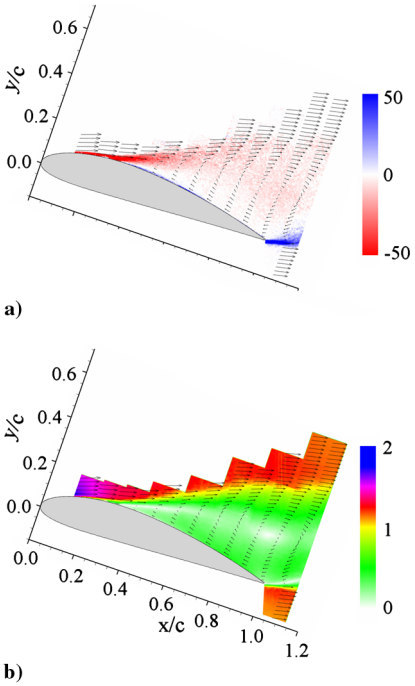

Fig. 5 Time-averaged raster plots of a) normalized spanwise vorticity $\hat{\omega}_z$ and b) velocity magnitude $\hat{v}$ in the baseline (stalled) flow.

the higher-speed side that accompanies the roll up of the severed clockwise (CW) vorticity concentration. This roll up continues and, by $t/T_{conv} = 0.6$ (Fig. 6d), the detached vortex appears to be rolled up and advected downstream (note that, unfortunately, the core of this vortex that is located at $x/c \approx 0.6$ and $y/c \approx 0.2$ is not fully captured by the data frames of Fig. 3).

Perhaps the most remarkable feature in these images is the evolution of the surface vorticity layer that appears to adhere to the surface and, by $t/T_{conv} = 0.8$ (Fig. 6e), begins to roll up along its downstream edge. This roll up is evident in the transport of higher-speed fluid toward the surface in the map (the core of the detached CW vortex is nominally at $x/c \approx 0.7$ and $y/c \approx 0.3$). This near-wall CW vorticity concentration continues to roll up as it is advected along the surface and, by $t/T_{conv} = 1$ (Fig. 6f), the velocity field shows two separate flow domains: namely, an (upstream) attached domain ($x/c < 0.55$) where the flow is nominally attached to the airfoil (and the outer flow is turned toward the airfoil) and a large recirculation domain farther downstream that is continuously advected toward the trailing edge. This trend continues at $t/T_{conv} = 1.4$ (Fig. 6g), where the attached CW vortex continues its roll up and protrusion into the crossflow while it is advected along the surface. The leading edge of the attached vortex reaches $x/c \approx 0.8$, and the extent of the separated domain is substantially diminished. At $t/T_{conv} = 2$ (Fig. 6h), the attached CW vortex begins to lift off the surface of the airfoil, and the separation point on the surface begins to migrate upstream as recirculating flow is induced by the vortex lifting along the surface. Although at $t/T_{conv} = 3.8$ (Fig. 6i) the vortex is completely lifted off the surface, the flow relaxation to the unforced stalled state is very slow. This slow detachment process is consistent with what has been observed previously when some steady-state stall-control actuation is terminated (see Darabi and Wygnanski [20,21], Siauw et al. [22], Mathis et al. [23]). It is remarkable, however, that a single pulse is sufficient to attach the flow over a substantial portion of the airfoil. As shown next, these time scales are also characteristic of the aerodynamic forces and moments that are associated with large-scale manipulation of these vorticity concentrations.

The relaxation time of the flow following the actuation is measured by the (vector) difference between cross-stream velocity

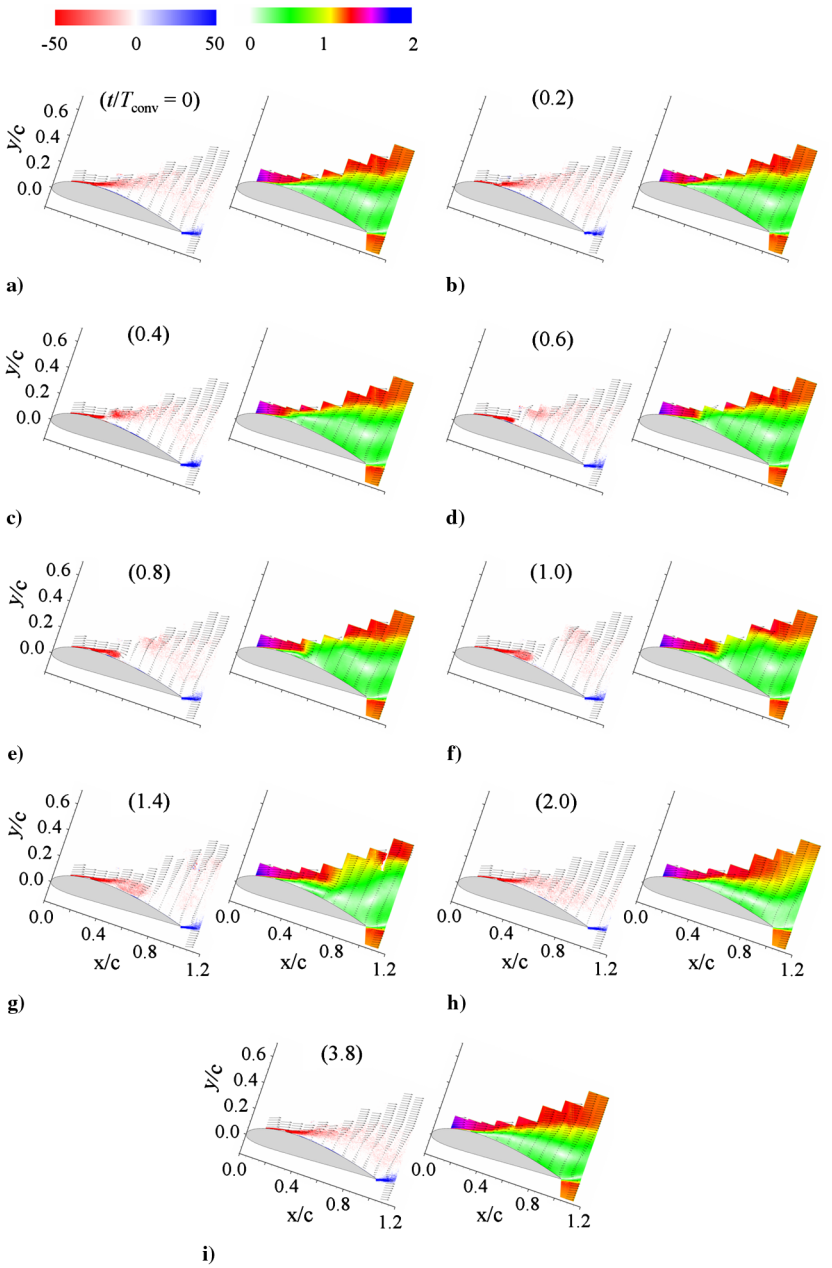

Fig. 6 Sequence of pairs of raster plots of normalized spanwise vorticity $\hat{\omega}_z$ (left) and velocity magnitude $\hat{v}$ (right) taken at t/T_{conv}= a) 0, b) 0.2, c) 0.4, d) 0.6, e) 0.8, f) 1, g) 1.4, h) 2, and i) 3.8 following the actuation.

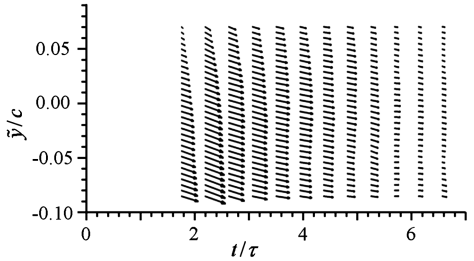

Fig. 7 Cross-stream distributions of the residual (resultant) vectors $\Delta\tilde{u} = \bar{U}(x,y) - \tilde{u}(x,y,t)$ at $\tilde{x}/c = 1$ and $-0.085 < \tilde{y}/c < 0.075$ for $1.8 < t/T_{\text{conv}} < 6.6$.

distributions of the stalled (unforced) flow and following actuation well above the airfoil (at $\tilde{x}/c = 1$ and $-0.085 < \tilde{y}/c < 0.075$) for $1.8 < t/T_{\text{conv}} < 6.6$. Cross-stream distributions of the residual (resultant) vectors, $\Delta\tilde{u} = \bar{U}(x,y) - \tilde{u}(x,y,t)$, are shown in Fig. 7. These distributions clearly show that, as a result of the actuation, the freestream above the airfoil is turned toward the airfoil, indicating a momentary increase in lift. These data also indicate that the relaxation time of the flow following the actuation is quite long compared with the convection time over the airfoil and is indicative of the response of the aerodynamic forces and moments to pulse actuation. It is conjectured that the relaxation time is associated with the reorganization of the vorticity concentrations on the top (suction) surface of the airfoil.

The evolution of the flowfield within the domain where the separating vorticity layer is severed from the surface of the airfoil as a result of the actuation was measured at shorter delay increments $\Delta(t/T_{\text{conv}}) = 0.025$ following the onset of actuation. These data were obtained in frame A (Fig. 3), which measures $0.15c \times 0.15c$ (the lower left edge is located at $x/c = 0.32$, i.e., $0.12c$ downstream of the actuator). Figures 8a–8f show a sequence of pairs of raster plots of $\hat{\omega}_z$ and $\hat{v}$ taken at six equally spaced time delays following the actuation. At $t/T_{\text{conv}} = 0.125$ (Fig. 8a), the (convective) effects of the

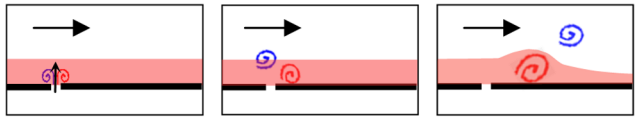

Fig. 9 Schematic rendition of the interaction of a spanwise counter-rotating vortex pair that is formed by a pulsed, momentary jet with a crossflow.

actuation have not reached this frame. The layer of separated CW vorticity is clearly visible, along with the formation of a CCW vorticity layer near the surface, owing to the reversed flow (note the white contour band $\hat{v} = 0$ that separates between the forward and reversed flows).

As shown by Vukasinovic et al. [35], and as shown schematically in Fig. 9, a momentary actuation jet in a crossflow results in the formation of a (spanwise) counter-rotating vortex pair that immediately begins to interact with the boundary layer. While the CW (right) vortex is advected within the boundary layer, the CCW (left) vortex is rotated around the CW vortex and is lifted into the freestream, where it is advected faster than the CW vortex within the boundary layer. This CCW vortex and its induced velocity are clearly visible in Fig. 8b ($t/T_{\text{conv}} = 0.2$) above the separated vorticity layer, but it seems to have minimal direct impact on the separated flow. At the same time, the effect of the CW vortex within the upstream boundary layer is already evident, in that the separation point, $\partial v/\partial n = 0$ (where n is the unit vector normal to the surface), is moved slightly downstream, and this motion is even more evident in Fig. 8c ($t/T_{\text{conv}} = 0.275$). Note that the CW vorticity layer in Fig. 8c is beginning to thin near the surface, and there is a thin protrusion of CW vorticity along the surface that is consistent with the downstream migration of the separation point (to $x/c \approx 0.37$). The severing of the separated vorticity layer by the CW actuation jet vortex is even more evident in Figs. 8d–8f ($t/T_{\text{conv}} = 0.35$–0.5). These data clearly demonstrate the demarcation between two flow domains, namely, the separated flow that is advancing downstream and a pseudo-attached flow, where the upstream vorticity layer along the surface is clearly

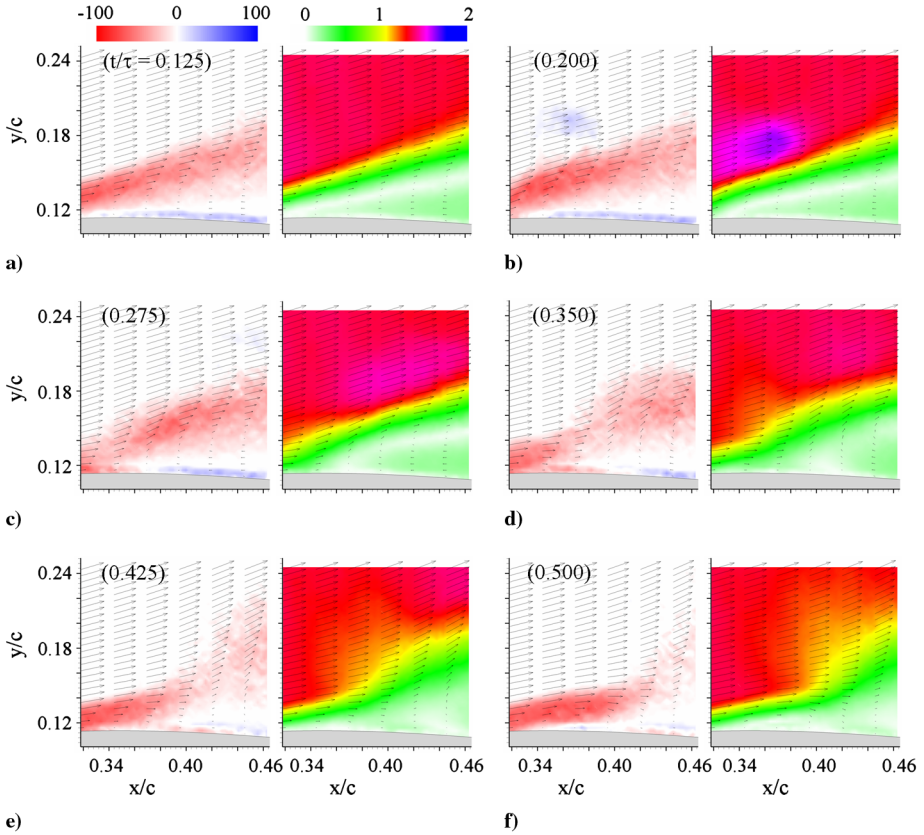

Fig. 8 A time sequence of pairs of raster plots of normalized spanwise vorticity $\hat{\omega}_z$ and normalized velocity magnitude $\hat{v}$ taken at six equally spaced time delays t/T_{conv} following the actuation (each delay is noted in parentheses).

bent along the surface but is not fully attached, as may be evident by the vorticity gap along the surface at $t/T_{\text{conv}} = 0.5$ (Fig. 8f).

The evolution of the separated vorticity layer is accompanied by induced transitory pressure gradients in the flow. These gradients are computed algebraically from the 2-D Navier–Stokes equations where the velocity time derivatives are computed from successive (phase averaged) images taken $0.025T_{\text{conv}}$ apart (the error associated with both the spatial and temporal velocity derivatives is estimated to be within 2–3% based on the velocity error from the PIV measurements). Figure 10 shows a time sequence of pairs of raster plots of the normalized spanwise vorticity concentrations ($|\hat{\omega}_z| > 20$) on the left and the normalized streamwise pressure gradient $\hat{p}_x = (\partial p/\partial x)c/\rho U_0^2$, where $\partial p/\partial x$ is the streamwise pressure gradient and ρ is the air density. These data show that the arrival of the CW vortex that is induced by the actuation jet within the boundary

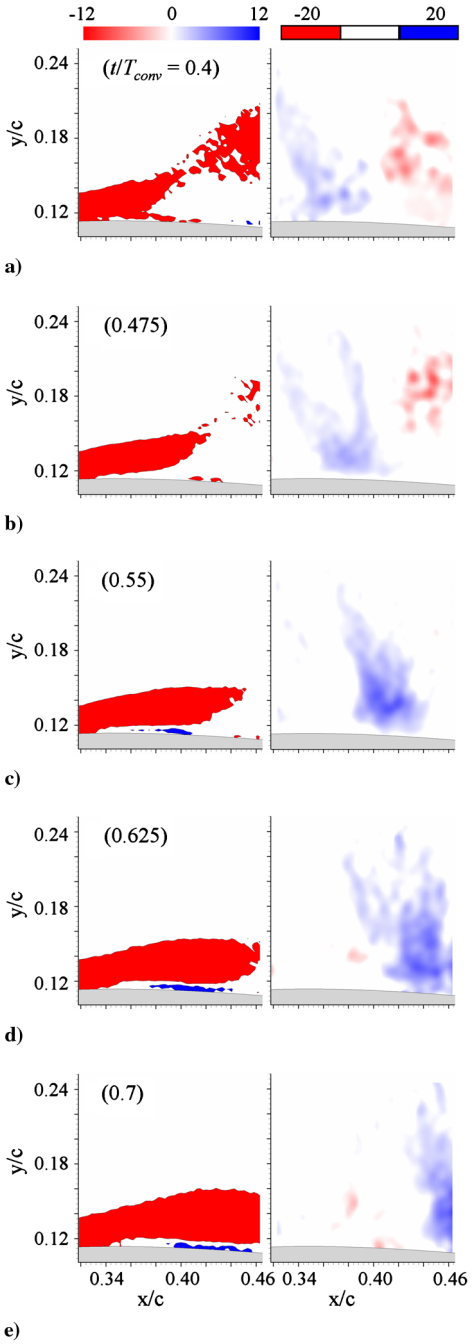

Fig. 10 Time sequence of pairs of raster plots of the spanwise vorticity concentrations ($|\hat{\omega}_z| > 20$) on the left and the normalized streamwise pressure gradient $\hat{p}_x$ on the right at t/T_{conv}= a) 0.4, b) 0.475, c) 0.55, d) 0.625, and e) 0.7.

layer (cf., Fig. 9) is accompanied by a localized (momentary) pressure rise that is characterized spatially by downstream and upstream favorable and adverse pressure gradients, respectively.

Figure 10a shows the onset of the severing of the separated vorticity layer by the CW actuation vortex. It is noteworthy that the favorable and adverse pressure gradient domains are roughly centered about the pinching zone, which widens as the favorable pressure gradient is advected downstream (Figs. 10b and 10c). The presence of the adverse pressure gradient (shown in blue) ahead of the leading edge of the surface vorticity layer apparently leads to a slight liftoff from the surface and the formation of a thin bubble of CCW vorticity concentration near the surface. It is interesting to note that the curvature that is imposed by the presence of this trapped CCW vortex enables the outer CW vorticity to bend toward the surface (Figs. 10d and 10e) rather than continue to separate from it. Earlier works (e.g., Glezer et al. [17]) have shown that the formation of such trapped vorticity concentrations can, in fact, delay separation of flows along curved surfaces. Finally, it is noted that the propagation velocity of the peak adverse pressure gradient is estimated to be $0.3U_0$.

The global effects of the actuation on the flow over the airfoil are assessed from measurements of the flowfield in the near wake. These measurements are presented in the laboratory frame of reference at $\tilde{x}/c = 1$ (cf., Fig. 1). Figure 11 shows cross-stream distributions of the normalized streamwise and cross-stream velocity components, $\hat{u}$ and $\hat{v}$, the spanwise vorticity, $\hat{\omega}_z$, and the turbulent kinetic energy, $\hat{k}$. These data are presented for the time-averaged unforced (baseline) flow (Fig. 11a), and they are phase averaged following the transitory actuation at $t/T_{\text{conv}} = 1$, 2, and 5 (Figs. 11b–11d, respectively). The (time-averaged) streamwise velocity in the base flow is reversed (with a minimum value of $\hat{u} = -0.37$) for $-0.12 < \tilde{y}/c < -0.01$, which corresponds to the two local peaks in the cross-stream velocity. As expected from Fig. 5a, the CCW (positive) spanwise vorticity is concentrated in the boundary layer of the pressure (bottom) side of the airfoil, while the CW (negative) vorticity that is associated with the separated flow over the suction (top) side of the airfoil is distributed over a much broader section of the wake. Also note the high levels of the turbulent kinetic energy in the reversed flow section of the wake. The data in Fig. 11 show that the effect of the actuation is most prominent at $t/T_{\text{conv}} = 2$ (Fig. 11c) and is manifested by reduction in the width and depth of the wake (the minimum velocity is $-0.1U_o$, and the wake width is reduced from $0.6c$ to $0.5c$), in the extent of the reversed flow region, and in the concentration of turbulent kinetic energy. The data in Fig. 11d ($T_{\text{conv}} = 5$) clearly show that, even after five convective time scales, the flow still has not fully returned to the unforced state.

The temporal variation of the aerodynamic characteristics of the airfoil under pulse actuation is assessed from measurements of the vorticity flux into the near wake, which is used to obtain an estimate of the global time rate of change of circulation. The vorticity flux into the wake and the time rate of change in circulation about the airfoil $\mathrm{d}\Gamma/\mathrm{d}t$ are computed based on a simple control volume analysis (this is similar in principle to the procedure used by Shih and Ho [36], except that the present analysis takes into account vorticity flux from both the top and bottom sides of the trailing edge). Once $\mathrm{d}\Gamma/\mathrm{d}t$ is calculated, $\Gamma(t)$ is computed by simple integration forward in time using a first-order Euler method. In these calculations, $\mathrm{d}\Gamma/\mathrm{d}t$ at some $t_{\text{ref}} = 0$ (i.e., before actuation is applied) is nominally zero (since there is no change in the time-averaged circulation). However, since the cross-stream width of the CCW vorticity layer (from the pressure surface) near the trailing edge of the airfoil is inherently much narrower than the corresponding layer of the CW vorticity (from the suction surface), the net vorticity flux at $t_{\text{ref}} = 0$ may be nonzero (or offset) by (say) $\Delta\Gamma_{\text{offset}}$, owing to limited resolution. The magnitude of $\Delta\Gamma_{\text{offset}}$ is typically small and, in the present measurements, the ratio of the peak change in circulation (induced by actuation) $\Delta\Gamma_{\text{peak}}$ to $\Delta\Gamma_{\text{offset}}$ is at least 30 or larger. To assess the changes in circulation that are induced by the actuation relative to the time-averaged circulation Γ_0, $\mathrm{d}\Gamma/\mathrm{d}t$ is set to zero at $t_{\text{ref}} = 0$ (i.e., before the onset of actuation and integration in time).

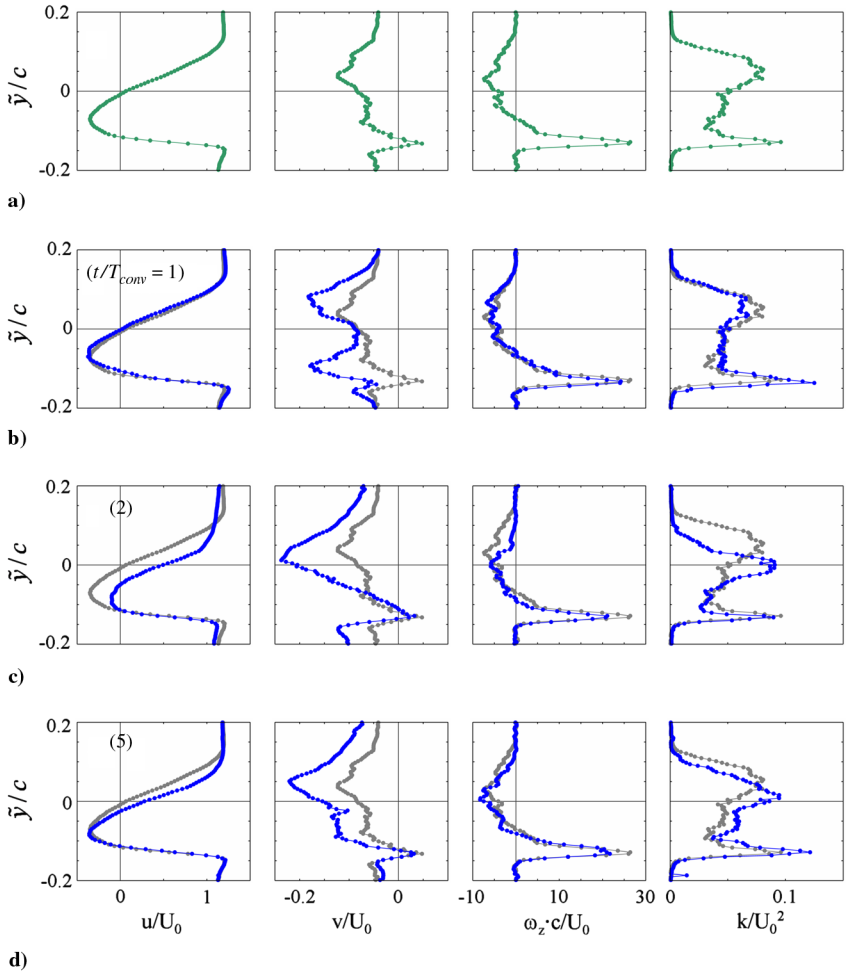

Fig. 11 Cross-stream distributions (from left to right) of the normalized streamwise and cross-stream velocity components $\hat{u}$ and $\hat{v}$, the spanwise vorticity $\hat{\omega}_z$, and the turbulent kinetic energy $\hat{k}$: a) the time-averaged unforced (baseline) flow and b) the phase averaged at $t/T_{\text{conv}} = 1$, c) 2, and d) 5. The baseline curves in a) are shown in gray in b)–d) for reference (Woo et al. [29]).

Figure 12 shows the temporal variation of the normalized vorticity flux (neglecting turbulent convection), $\hat{F}_\omega = (1/U_0^2) \int \bar{u}\bar{\omega}_z \, d\tilde{y}$, across the two domains within the wake that are distinguished by the separate CW and CCW vorticity concentrations shed from the top and bottom surfaces, respectively [as defined by the global change in sign between CCW (positive) and CW (negative) vorticity]. Also included is the time trace of the overall (net) vorticity flux into the wake. The vorticity flux from the top surface of the airfoil shows evidence of the shedding of the detached (or severed) CW vortex that is associated with the stalled flow (Fig. 6h). The passage of this vortex leads to negative flux beginning at $t/T_{\text{conv}} = 0.8$. Following a local peak at $t/T_{\text{conv}} = 1.2$, there is a decrease in the (negative) flux from the top surface and, at $t/T_{\text{conv}} = 1.8$, the magnitude of the vorticity flux from the top surface is temporarily slowed, indicating accumulation. However, since during this time the (positive) vorticity flux from the bottom surface of the airfoil continues at an almost time invariant rate, the net vorticity flux (from both surfaces) first undergoes a momentary decrease that is followed by an increase, which indicates corresponding decrease and increase in circulation (and potentially in lift). For $t/T_{\text{conv}} > 1.8$, the negative vorticity flux from the top surface slowly recovers (as the vorticity layer on the top surface begins to grow and lift off the surface; cf., Figs. 6g–6i), indicating that the circulation begins to decrease. For $t/T_{\text{conv}} > 2.3$, as the flow begins to return to its stalled state (cf., Fig. 6i), the vorticity flux asymptotically becomes zero, indicating no further changes in circulation. One of the noteworthy features of Fig. 12 is that the global temporal changes induced by the pulse actuation primarily affect the vorticity flux from the top surface while the adjustments to the flux at the bottom surface appear to be almost negligible.

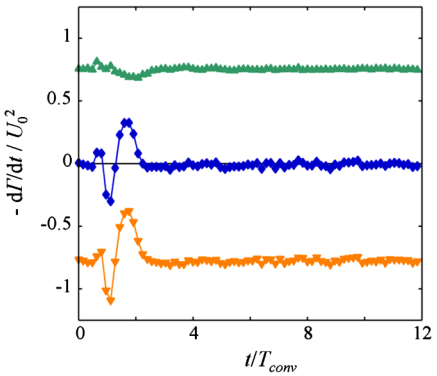

Fig. 12 The temporal variation of the normalized vorticity flux $\hat{F}_\omega$: CW (from top, ▼), CCW (from bottom, ▲), and their sum (◆) (Woo et al. [29]).

Figure 13 shows the normalized increment in circulation relative to the unforced (stalled) flow, $-\Delta\Gamma/\Gamma_0$. Note that, during the shedding of the CW vorticity from the stalled domain ($1.1 < t/T_{\text{conv}} < 1.3$), the magnitude of circulation about the airfoil decreases by about 12%. Once this shedding is complete, the ensuing positive vorticity flux (cf., Fig. 11) leads to a recovery in circulation to a level that is about 25% greater than the baseline (stalled) level at $t/T_{\text{conv}} = 2.3$. As noted in connection with Fig. 12, for $t/T_{\text{conv}} > 2.3$, the circulation begins to decrease monotonically as the flow returns to the fully stalled state. As discussed previously, it is remarkable that the decrease in circulation occurs over several convective time scales

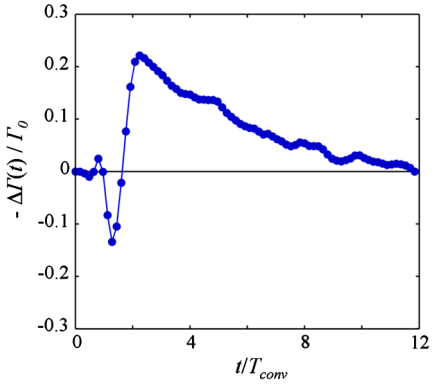

Fig. 13 The normalized increment in circulation $-\Delta\Gamma/\Gamma_0$ relative to the unforced (stalled) flow (Woo et al. [29]).

(as shown in Fig. 13, this process is finally complete at $t/T_{\text{conv}} = 8$), which suggests that attachment is faster than the subsequent separation, since these processes are driven by favorable and adverse pressure gradients, respectively. It is noteworthy that Darabi and Wygnanski [20,21] reported somewhat longer and significantly closer attachment and separation times over a flat-plate flap configuration (16 and $21T_{\text{conv}}$, respectively, scaled with the flap length). The dynamics of the attachment and separation suggest that the mechanisms of formation, advection, and subsequent detachment of the vorticity layer from the top surface have elements that are similar to that of dynamic stall and can be exploited for maneuvers effected by flow control.

Finally, the variation in time (following the actuation) of the incremental changes (relative to the unforced flow) in the phase-averaged streamwise and cross-stream momentum fluxes into the wake (neglecting turbulent convection), $\Delta\hat{T}_{\tilde{x}} = \int \bar{u}^2\, \mathrm{d}\tilde{y}/(\frac{1}{2}U_0^2 c)$ and $\Delta\hat{T}_{\tilde{y}} = \int \bar{u}\,\bar{v}\, \mathrm{d}\tilde{y}/(\frac{1}{2}U_0^2 c)$, respectively, are shown in Fig. 14. The changes in these momentum fluxes may be thought of as representative of part of the overall changes in streamwise and cross-stream forces on the airfoil during the highly unsteady response of the flow to transitory actuation. While these terms represent only part of the fluxes in the momentum equations, given that the largest changes in flux between the baseline and various stages of reattachment occur in the wake, they provide an indicator of the respective changes in streamwise and cross-stream forces. The actuation-induced changes in the streamwise momentum flux $\Delta T_{\tilde{x}}$ suggest a momentary increase in drag during the shedding of the CW detached vortex (when there is also a reduction in circulation), followed by a decrease in drag when the vorticity layer migrates along the suction side of the airfoil. Concomitantly, $\Delta T_{\tilde{y}}$ first increases, suggesting a decrease in the upward force on the airfoil when there is a decrease in circulation, and then increases, suggesting a recovery of the upward force on the airfoil when the circulation increases (cf., Fig. 13).

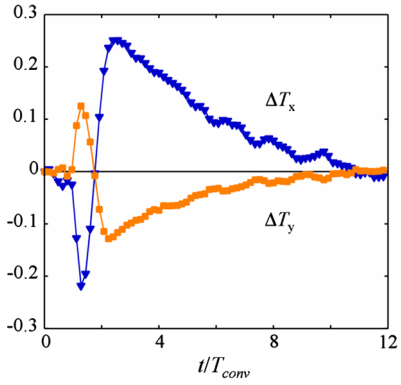

Fig. 14 The time variation of the incremental changes (relative to the unforced flow) in the streamwise and cross-stream momentum fluxes into the wake: $\Delta T_{\tilde{x}}/[(1/2)U_0^2 c]$ (▼) and $\Delta T_{\tilde{y}}/[(1/2)U_0^2 c]$ (■) (Woo et al. [29]).

IV. Conclusions

The receptivity of the separated flow over a stalled airfoil to pulse actuation is investigated experimentally. The actuation results in transitory flow attachment and large-scale changes in vorticity accumulation and flux and, consequently, changes in the global circulation and aerodynamic forces. In the present experiments, actuation is applied by a momentary [$\mathcal{O}$(1 ms)] jet produced by a combustion-based actuator, such that the characteristic duration of the impulse is on a time scale that is an order of magnitude shorter than the characteristic convective time over the airfoil. The flowfield in the cross-stream plane above the airfoil and in its near wake is measured with multiple high-resolution PIV images that are obtained phase locked to the actuation, allowing for continuous tracking of vorticity concentrations.

The dynamics of the separated flow domain are drastically altered when actuation is applied. The actuation results in two prominent effects. First, the separated vorticity layer is severed from the surface of the airfoil, and a detached large-scale CW vortex is formed and advected away from the airfoil. The second effect is the formation and advection of a CW vorticity layer along the surface of the airfoil that ultimately begins to roll up along its leading edge before lifting off the surface. While the shedding of the separated vorticity concentration occurs on one to two convective time scales, the formation and ultimate liftoff of the vorticity layer take considerably longer, on the order of 8 to 10 convective time scales. Detailed PIV measurements in the flow domain where the severing of the separated vorticity layer takes place indicate that the actuation jet forms a counter-rotating vortex pair. While the CCW vortex is ejected into and advected by the crossflow, the CW vortex remains within the boundary layer and induces a localized domain of favorable streamwise pressure gradient that is followed by a similar domain of an adverse gradient. The pressure peak between these domains is centered about the location of the separated vorticity layer breakup. It is conjectured that the adverse pressure gradient leads to the onset of accumulation of vorticity near the upstream edge of the surface layer, which continues to move along the surface but is not attached to it and ultimately lifts off.

The global effects of the actuation on the flow over the airfoil are assessed from measurements of the flowfield in the near wake. The temporal variation of the aerodynamic characteristics of the airfoil under pulse actuation is assessed from measurements of the vorticity flux into the near wake, which is used to obtain the global time rate of change of circulation. The present measurements show that virtually all the transitory vorticity flux is associated with the top (suction) side of the airfoil while the shedding of (positive) vorticity from the bottom surface is nearly invariant. The vorticity flux from the top surface of the airfoil shows evidence of the shedding of the detached (or severed) CW vortex that is associated with the stalled flow. The shedding of this vortex leads to an increase in negative vorticity flux and, therefore, to a momentary decrease in circulation. However, the formation and advection of the surface vorticity layer results in accumulation of CW vorticity and a decrease in vorticity flux from the top surface while the bottom surface continues to shed positive (CCW) vorticity that leads to an increase of up to 25% in circulation (and potentially in lift) compared with the baseline (stalled) flow. As the CW vorticity layer on the top surface begins to lift off, the vorticity flux from the top surface increases until, ultimately, the net flux vanishes when the flow is fully stalled again.

As discussed previously, it is remarkable that the decrease in circulation occurs over several convective time scales, suggesting that the mechanisms of formation, advection, and subsequent detachment of the vorticity layer from the top surface has elements that are similar to that of dynamic stall and can be exploited for maneuvers effected by flow control.

Acknowledgment

This work has been supported by the U. S. Air Force Office of Scientific Research–Multidisciplinary Research Initiative.

References

[1] Wu, J.-Z., Lu, X.-Y., Denny, A. G., Fan, M., and Wu, J.-M., "Post Stall Flow Control on an Airfoil by Local Unsteady Forcing," *Journal of Fluid Mechanics*, Vol. 371, 1998, pp. 21–58. doi:10.1017/S0022112098002055

[2] Ahuja, K. K., and Burrin, R. H., "Control of Flow Separation by Sound," 9th Aeroacoustics Conference, AIAA Paper 1984-2298, 1984.

[3] Neuburger, D., and Wygnanski, I., "The Use of a Vibrating Ribbon to Delay Separation on Two Dimensional Airfoils," *Proceedings of Air Force Academy Workshop in Unsteady Separated Flow*, U. S. Air Force Academy TR-88-0004, Colorado Springs, CO, 1987.

[4] Seifert, A., Darabi, A., and Wygnanski, I., "Delay of Airfoil Stall by Periodic Excitation," *Journal of Aircraft*, Vol. 33, No. 4, 1996, pp. 691–698. doi:10.2514/3.47003

[5] Tuck, A., and Soria, J., "Active Flow Control over a NACA 0015 Airfoil using a ZNMF Jet," 15th Australasian Fluid Mechanics Conference, Univ. of Sydney, Paper AFMC00178, Sydney, Australia, 2004.

[6] Sosa, R., Artana, G., Moreau, E., and Touchard, G., "Flow Control with EHD Actuators in Middle Post Stall Regime," *Journal of the Brazilian Society of Mechanical Sciences and Engineering*, Vol. 28, No. 2, 2006, pp. 200–207. doi:10.1590/S1678-58782006000200009

[7] Wake, B. E., and Lurie, E. A., "Computational Evaluation of Directed Synthetic Jets for Dynamic Stall Control," 57th Annual Forum of the American Helicopter Society, American Helicopter Society, Paper A02-12351 01-05, Alexandria, VA, 2001.

[8] Duraisamy, K., and Baeder, J. D., "Active Flow Control Concepts for Rotor Airfoils using Synthetic Jets," 1st AIAA Flow Control Conference, AIAA Paper 2002-2835, 2002.

[9] Florea, R., and Wake, B. E., "Parametric Analysis of Directed-Synthetic Jets for Improved Dynamic-Stall Performance," 41st AIAA Aerospace Sciences Meeting and Exhibit, AIAA Paper 2003-216, 2003.

[10] Lorber, P. F., McCormick, D. C., Anderson, T., Wake, B., MacMartin, D., Pollack, M., Corke, T., and Breuer, K., "Rotorcraft Retreating Blade Stall Control," AIAA Fluids 2000 Conference and Exhibit, AIAA Paper 2002-2475, 2000.

[11] Lorber, P. F., McCormick, D. C., Wake, B., and Florea, R., "Separation Control for Rotorcraft," United Technologies Research Center Final Progress Rept. 2002-5.200.0015-5, East Hartford, CT, 2002.

[12] Greenblatt, D., and Wygnanaski, I., "Dynamic Stall Control by Periodic Excitation, Part 1: NACA 0015 Parametric Study," *Journal of Aircraft*, Vol. 38, No. 3, 2001, pp. 430–438. doi:10.2514/2.2810

[13] Smith, B. L., and Glezer, A., "The Formation and Evolution of Synthetic Jets," *Physics of Fluids*, Vol. 10, No. 9, 1998, pp. 2281–2297. doi:10.1063/1.869828

[14] Honohan, A., Amitay, M., and Glezer, A., "Aerodynamic Control Using Synthetic Jets," Fluids 2000 Conference and Exhibit, AIAA Paper 2000-2401, 2000.

[15] Amitay, M., Smith, D. R., Kibens, V., Parekh, D. E., and Glezer, A., "Aerodynamic Flow Control over an Unconventional Airfoil Using Synthetic Jet Actuators," *AIAA Journal*, Vol. 39, No. 3, 2001, pp. 361–370. doi:10.2514/2.1323

[16] Amitay, M., and Glezer, A., "Controlled Transients of Flow Reattachment over Stalled Airfoils," *International Journal of Heat and Fluid Flow*, Vol. 23, No. 5, 2002, pp. 690–699. doi:10.1016/S0142-727X(02)00165-0

[17] Glezer, A., Amitay, M., and Honohan, A., "Aspects of Low- and High-Frequency Actuation for Aerodynamic Flow Control," *AIAA Journal*, Vol. 43, No. 7, 2005, pp. 1501–1511. doi:10.2514/1.7411

[18] Amitay, M., and Glezer, A., "Aerodynamic Flow Control of a Thick Airfoil Using the Synthetic Jet Actuators," *Proceedings of the 3rd ASME/JSME Joint Fluids Engineering Conference* [CD-ROM], American Society of Mechanical Engineers, Fairfield, NJ, 1999.

[19] Amitay, M., and Glezer, A., "Flow Transients Induced on a 2D Airfoil by Pulse-Modulated Actuation," *Experiments in Fluids*, Vol. 40, No. 2, 2006, pp. 329–331. doi:10.1007/s00348-005-0069-6

[20] Darabi, A., and Wygnanski, I., "Active Management of Naturally Separated Flow over a Solid Surface, Part 1: The Separation Process," *Journal of Fluid Mechanics*, Vol. 510, 2004a, pp. 131–144. doi:10.1017/S0022112004009243

[21] Darabi, A., and Wygnanski, I., "Active Management of Naturally Separated Flow over a Solid Surface, Part 2: The Forced Reattachment Process," *Journal of Fluid Mechanics*, Vol. 510, 2004b, pp. 105–129. doi:10.1017/S0022112004009231

[22] Siauw, W. L., Bonnet, J. P., Tensi, J., and Cattafesta, L. N., "Physics of Separated Flow over a NACA 0015 Airfoil and Detection of Flow Separation," 47th AIAA Aerospace Sciences Meeting, AIAA Paper 2009-144, 2009.

[23] Mathis, R., Lebedev, A., Collin, E., Delville, J., and Bonnet, J.-P., "Experimental Study of Transient Forced Turbulent Separation and Reattachment of a Beveled Trailing Edge," *Experiments in Fluids*, Vol. 46, No. 1, 2009, pp. 131–146. doi:10.1007/s00348-008-0549-6

[24] Crittenden, T., Glezer, A., Funk, R., and Parekh, D., "Combustion-Driven Jet Actuators for Flow Control," 31st Fluid Dynamics Conference and Exhibit, AIAA Paper 2001-2768, 2001.

[25] Crittenden, T., Schlyubcky, D., and Glezer, A., "Combustion-Driven Jet Actuators in Reversed Flow Configurations," 2nd Flow Control Conference, AIAA Paper 2004-2689, 2004.

[26] Crittenden, T., Warta, B. J., and Glezer, A., "Characterization of Combustion Powered Actuators for Flow Control," 3rd Flow Control Conference, AIAA Paper 2006-2864, 2006.

[27] Funk, R., Parekh, D., Crittenden, T., and Glezer, A., "Transient Separation Control Using Pulsed Combustion Actuation," 1st Flow Control Conference, AIAA Paper 2002-3166, 2002.

[28] Brzozowski, D., and Glezer, A., "Transient Separation Control using Pulse-Combustion Actuation," 3rd AIAA Flow Control Conference, AIAA Paper 2006-3024, 2006.

[29] Woo, G. T. K., Crittenden, T. M., and Glezer, A., "Transitory Control of a Pitching Airfoil using Pulse Combustion Actuation," 4th AIAA Flow Control Conference, AIAA Paper 2008-4324, 2008.

[30] Woo, G. T. K., Crittenden, T. M., and Glezer, A., "Transitory Separation Control over a Stalled Airfoil," 39th AIAA Fluid Dynamics Conference, AIAA Paper 2009-4281, 2009.

[31] Woo, G. T. K., and Glezer, A., "Transient Control of the Separating Flow over a Dynamic Airfoil," 48th AIAA Aerospace Sciences Meeting, AIAA Paper 2010-861, 2010.

[32] Abbott, I. H., and von Doenhoff, A. E., *Theory of Wing Sections*, Dover, New York, 1959.

[33] Adrian, R. J., "Particle-Imaging Techniques for Experimental Fluid Mechanics," *Annual Review of Fluid Mechanics*, Vol. 23, No. 1, 1991, pp. 261–304. doi:10.1146/annurev.fl.23.010191.001401

[34] Westerweel, J., "Theoretical Analysis of the Measurement Precision in Particle Image Velocimetry," *Experiments in Fluids*, Vol. 29, No. 7, 2000, pp. S003–S012. doi:10.1007/s003480070002

[35] Vukasinovic, B., Lucas, D. G., and Glezer, A., "Controlled Manipulation of Small- and Large-Scales in a Turbulent Shear Layer, Part I: Experimental Studies," 35th Fluid Dynamics Conference and Exhibit, AIAA Paper 2005-4753, 2005.

[36] Shih, C., and Ho, C.-M., "Vorticity Balance and Time Scales of a Two-Dimensional Airfoil in an Unsteady Free Stream," *Physics of Fluids*, Vol. 6, No. 2, 1994, pp. 710–723. doi:10.1063/1.868310

A. Naguib
Associate Editor